Microsyst Technol (2013) 19:577–582
DOI 10.1007/s00542-012-1660-4

TECHNICAL PAPER

A water-immersible 2-axis scanning mirror microsystem for ultrasound andha photoacoustic microscopic imaging applications

Chih-Hsien Huang · Junjie Yao · Lihong V. Wang · Jun Zou

Received: 10 July 2012 / Accepted: 23 August 2012 / Published online: 13 September 2012

Abstract Fast scanning is highly desired for both ultrasound and photoacoustic microscopic imaging, whereas the liquid environment required for acoustic propagation limits the usage of traditional microelectromechanical systems (MEMS) scanning mirrors. Here, a new water-immersible scanning mirror microsystem has been designed, fabricated and tested. To achieve reliable underwater scanning, flexible polymer torsion hinges fabricated by laser micromachining were used to support the reflective silicon mirror plate. Two efficient electromagnetic microactuators consisting of compact RF choke inductors and high-strength neodymium magnet disc were constructed to drive the silicon mirror plate around a fast axis and a slow axis. The performance of this water-immersible scanning mirror microsystem in both air and water were tested using the laser tracing method. For the fast axis, the resonance frequency reached 224 Hz in air and 164 Hz in water, respectively. The scanning angles in both air and water under ±16 V DC driving were ±12°. The scanning angles in air and water under ±10 V AC driving (at the resonance frequencies) were ±13.6° and ±10°. For the slow axis, the resonance frequency reached 55 Hz in air and 38 Hz in water, respectively. The scanning angles in both air and water under ±10 V DC driving were ±6.5°. The scanning angles in air and water under ±10 V AC driving (at the resonance frequencies) were ±8.5° and ±6°. The feasibility of using such a water-immersible scanning mirror microsystem for scanning ultrasound microscopic imaging has been demonstrated with a 25-MHz ultrasound pulse/echo system and a target consisting of three optical fibers.

C.-H. Huang (✉) · J. Zou
Department of Electrical and Computer Engineering, Texas A&M University, College Station, TX 77843, USA
e-mail: isaachuang0210@gmail.com

J. Zou
e-mail: junzou@tamu.edu

J. Yao · L. V. Wang
Optical Imaging Laboratory, Department of Biomedical Engineering, Washington University in St. Louis, St. Louis, MO 63130, USA

1 Introduction

Scanning mirrors have been used in a number of high-resolution optical imaging modalities, including optical coherence tomography (Hagelin et al. 2000; Yang et al. 2006), confocal microscopy (Hyejun et al. 2007) and multi-photon microscopy (Jung et al. 2008). Compared with conventional scanning mirrors (Liu 2006), microelectromechanical systems (MEMS) scanning mirrors have a smaller form factor and can provide higher scanning speeds. They are especially suitable for developing compact imaging probes for handheld, endoscopic and even intravascular applications. Currently, MEMS scanning mirrors are mainly designed for free-space optical beam steering in air, where the mirror supporting structure is made of brittle silicon-based material and the mirror is driven by delicate microactuators (Liu 2006). However, these designs are not suitable for underwater scanning operations in ultrasound (Chen et al. 2000) and photoacoustic imaging (Wang 2009; Wang et al. 2011; Yao et al. 2011; Yao and Wang 2011), where water is usually the matching medium for acoustic propagation (Fig. 1). For example, when immersed in water, the silicon supporting structures are susceptible to permanent damage from a small turbulence, shock or unbalanced surface tension force, which otherwise are often encountered in a liquid environment. Second, significant degradation in the scanning performance (e.g., maximal scanning angle and frequency) or complete

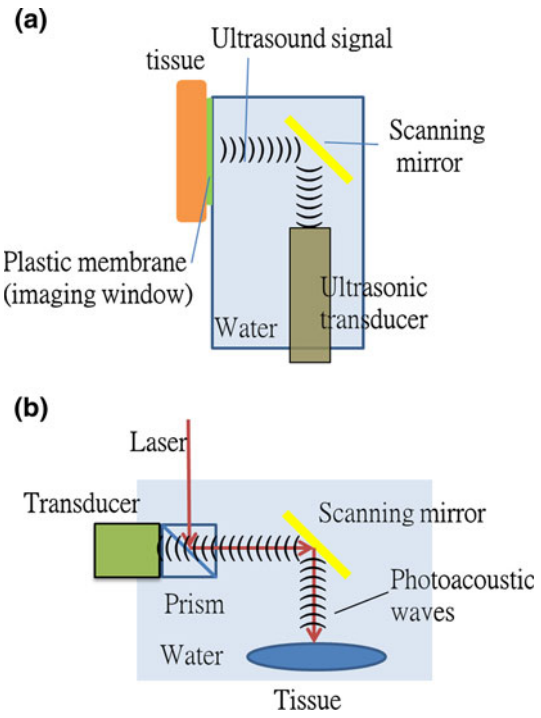

Fig. 1 Illustration of the underwater operation of micro scanning mirrors in **a** pulse-echo ultrasound and **b** photoacoustic microscopic imaging

device failure could occur due to electrical shorting, excessive cooling and fluidic damping. To address this issue, we report the development of a new water-immersible scanning mirror microsystem, which can reliably operate in both air and water. By utilizing high-strength polymer supporting materials and efficient electromagnetic microactuators, fast scanning of both optical and high-frequency ultrasonic beams in water has been successfully achieved. This new capability could enable the development of compact ultrasonic and photoacoustic microscopic imaging systems with fast imaging speed and large field of view.

2 Design and fabrication

2.1 Design

Figure 2a shows the schematic design of the water-immersible scanning mirror, which consists of a fast-axis module and a slow-axis module. The reflective mirror plate is housed in the fast-axis module and supported by two micro torsion hinges made of high-strength biaxially-oriented polyethylene terephthalate (BOPET) film. The low stiffness and high fracture strain of the polymer hinges help to reduce the required driving force and minimize the chance of shock damage (Liu 2006). Electromagnetic actuation was chosen as the driving mechanism to enable reliable underwater scanning. Compared with other microactuation mechanisms, such as electrostatic, piezoelectric and thermal methods, electromagnetic actuation does not need high voltage or electro-heating, and therefore is more suitable in a liquid environment. Compact electromagnetic actuation was achieved by combining a single inductor coil with two micro rare-earth magnet discs attached to the two ends of the mirror plate with opposite polarities. When an AC or DC current flows through the inductor coil, the resultant magnetic field creates a torque on the magnets and thus rotates the mirror plate around the torsional supporting hinges. To achieve the second (slow) axis scanning, the fast-axis module is attached to the slow-axis module with the support of two BOPET torsional hinges (Fig. 2b). Four inductor coils and four micro rare-earth magnet discs were arranged into two groups with opposite polarities to provide the torsional driving force for the slow-axis scanning. Due to its larger mass, the resonant frequency of the slow-axis module will be lower than the fast-axis module. One advantage of the above modular design is that scanning motion in the two axes is largely decoupled, which helps to improve the scanning accuracy, linearity and repeatability.

In ultrasound and photoacoustic imaging, the optical and ultrasound signals are in the form of short pulses with a typical repetition rate of kHz. To maintain a dense pixel formation, the scanning frequency of the scanning mirror should be 10 to 100 s of Hz. A maximal scanning angle larger than 10° is desirable to provide a good field of view. To ensure a good numerical aperture, the size of the mirror plate should be as large as possible. In addition, the driving voltage needed to be minimized to reduce the risk of electrical shorting and shock especially in water. Tables 1 and 2 list the main design parameters of the fast-axis and slow-axis module. Based on these design parameters, a preliminary mechanical analysis was conducted to provide a first-order estimation of their scanning performances (scanning angle, resonant frequency and driving voltage). The magnetic force (F) generated between the permanent magnet discs and the inductor coil can be determined by

$$F = \mathrm{V} \times \mathrm{Ms} \times \frac{\partial \mathrm{H}}{\partial \mathrm{z}}, \tag{1}$$

where V is the volume of permanent magnetic disc, Ms is the magnetization of the magnet disc. H is the magnetic field intensity generated by inductor. The torque T_{mag} generated by the magnetic force and the resulting rotation angle (ϕ) can be determined by

$$T_{mag} = \mathrm{F} \times \mathrm{L}', \tag{2}$$

$$\phi = \frac{TL}{JG}, \tag{3}$$

where L, J and G are the length, torsional moment of inertia and shear modulus of elasticity of the BOPET hinges, respectively and L' is the work distance between the magnetic force (F) and the BOPET hinges. For the BOPET

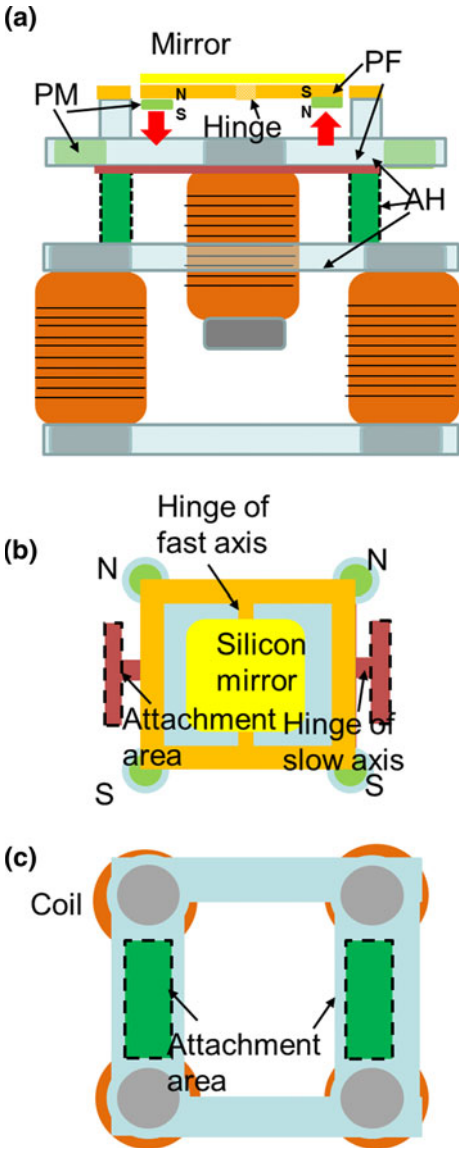

Fig. 2 Schematics of the water-immersible scanning mirror design: **a** *side view*; **b** *top view* of fast-axis module; and **c** *top view* of slow-axis module. *PM* permanent magnets, *PF* polymer frame, *AF* actuation force, *AH* acrylic holder

hinge with a rectangular cross-section, the torsion moment of inertia (J) can be determined by

$$\mathrm{J} = \mathrm{w}t^3\left[\frac{16}{3} - 3.36\frac{t}{w}\left(1 - \frac{t^4}{12w^4}\right)\right], \tag{4}$$

where w is the width and t is the thickness of the BOPET hinge. The resonant frequency in air (f_{r_air}) of the fast-axis and the slow-axis modules can be estimated by

$$f_{r\_air} = \frac{1}{2\pi}\sqrt{\frac{K^*}{m}}, \tag{5}$$

where K^* is the torsional force constant of the BOPET hinge and m is the overall effective mass of the fast-axis and the slow-axis modules, respectively. Due to the small movement of the mirror plate during scanning and the relatively large mass of the two modules, the damping from the air can be neglected. When the scanning mirror is immersed in water, the resonant frequency (f_{r_water}) can be estimated by

$$f_{r\_water} = f_{r\_air}\sqrt{1 + \frac{3\pi\rho b}{2\rho_m t'}}^{-1}\ \Gamma_t(k), \tag{6}$$

where ρ is the density of water, ρ_m and b are the effective density and width of the scanning mass, $\Gamma_t(k)$ is hydrodynamic functions, and k is normalized mode numbers (Cornelis and John 2006). From Eqs. (1)–(6), the estimated scanning angles and resonant frequencies of the fast-axis and slow-axis modules are listed in Table 3.

2.2 Fabrication

The fabrication of the water-immersible scanning mirror was conducted as follows. First, the reflective mirror plate (9×9 mm^2) was diced from a polished single-crystalline silicon substrate. The polished silicon substrate provides

Table 1 Design parameters of the fast-axis module

Inductor		Neodymium magnets	
Inductance	33 mH	Thickness	0.8 mm
		Diameter	3.125 mm
Mirror plate		Supporting hinge	
Length	9 mm	Length	1 mm
Width	9 mm	Width	0.9 mm
Thickness	500 μm	Thickness	75 μm

Table 2 Design parameters of slow-axis module

Inductor		Neodymium magnets	
Inductance	33 mH	Thickness	1.6 mm
		Diameter	3.125 mm
Mirror Plate		Supporting Hinge	
Length	9 mm	Length	1 mm
Width	9 mm	Width	1.4 mm
Thickness	500 μm	Thickness	75 μm

Table 3 Estimated driving angles and resonance frequencies

	Fast axis		Slow axis
ϕ (DC 16 V)	12.8°	ϕ (DC 10 V)	7.88°
f_{r_air}	214.38 Hz	f_{r_air}	63.92 Hz
f_{r_water}	160.06 Hz	f_{r_water}	45.24 Hz

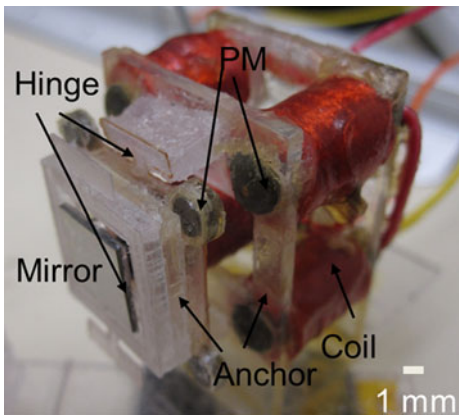

Fig. 3 A fully assembled prototype of the water-immersible scanning mirror

excellent surface smoothness and flatness, and also good acoustic reflectivity due to the large acoustic impedance mismatch between silicon (19.6×10^6 N s/m^3) and water (1.47×10^6 N s/m^3). A thin layer of gold coating ($\sim$70 nm thick) was deposited onto the silicon mirror surface using e-beam evaporation to enhance its optical reflectivity. Second, the BOPET torsional hinges and acrylic holders of both fast-axis and slow-axis modules were made by using a laser cutting machine. During the assembly, the silicon mirror plate, the BOPET torsional hinges, the permanent magnet discs (D21B-N52, K&J Magnetics), the inductor coil (70F331AF-RC, BOURNS) and the acrylic holder were assembled and bonded together with silicone rubber adhesive (RTV 108, Momentive Performance Materials) to form the fast-axis module. The same procedure was repeated to make the slow-axis module. Finally, the fast-axis module was bonded onto the acrylic holder of the slow-axis module (see Fig. 2). After insulating the coils and electrical connections, the entire 2-D scanning mirror module can be immersed in water to ensure a reliable underwater scanning operation (Fig. 3).

3 Characterization

The scanning angle ϕ and resonance frequency f_r of the scanning mirror were measured in air and water by using the laser tracing method (Fig. 4). During the measurement, the scanning mirror was mounted on the bottom of a water tank. A ruler was placed 6.5 cm away from the center of the mirror plate at an angle of 45°. The laser beam from a laser pointer was projected onto the mirror plate with an incident angle of 45° and reflected onto the ruler. The scanning angle was calculated based on the trace of the laser beam on the ruler. To determine the resonance frequency, an AC driving voltage with varied frequency was applied. The resonance frequency is defined as the frequency of the AC driving voltage when the scanning angle reaches its maximum. Figure 5 shows the scanning angles of the fast axis under DC and AC driving conditions. As shown in Fig. 5a, under DC driving condition, the scanning angle increased with the driving voltage in both directions [clockwise (CW) and counter-clockwise (CCW)]. The scanning angle reached 12° with a 16 V driving voltage, which matches well with the estimated value. The scanning angles of the fast axis were similar in air and water. This is because the mirror plate was driven in a quasi-static mode and the dynamic damping from water can be negligible. As shown in Fig. 5b, with AC driving at the resonance frequency, the scanning angle increased with the peak driving voltage in both air and water. However, due to the dynamic damping in water, the resonance frequency drops from 224 Hz in air to 164 Hz in water, which is similar to the estimation results and higher driving voltage is needed to maintain the same scanning angle. For example, at a scanning angle of 10°, the required peak driving voltage increased from 7.5 V in air to 10 V in water. The scanning performance of the slow axis of the scanning mirror was also characterized. As shown in Fig. 6a, under DC driving condition, the scanning angle reached 6.5° with a 10 V driving voltage in both air and water. The resonant frequency dropped from 55 Hz in air to 38 Hz in water. With an AC driving voltage of 10 volt (at 55 Hz in air and 38 Hz in water), the scanning angle dropped from 8.5° in air to 6° in water as shown in Fig. 6b. The estimated rotation angle and resonance frequencies of slow axis are not accurate as fast axis since the structure of the slow axis is much more complex, which is well described by a lumped-element model. In addition, as a reliability test, the fast axis of the scanning mirror was driven in water with a peak driving voltage of 10 V and a frequency of 164 Hz for over ten million cycles. No noticeable degradation in the scanning performance was observed.

4 Ultrasound imaging experiment

Using the water-immersible scanning mirror to steer focused ultrasound beam in water, pulse-echo ultrasound microscopic imaging of an optical-fiber target were successfully demonstrated. As shown in Fig. 7a, the imaging setup includes a water tank, a high-frequency (25 MHz) focused transducer with a focal length of 19 mm (V324N-SU, Olympus), the water-immersible scanning mirror, and three optical fibers as the imaging target. The scanning mirror is placed 9 mm away from the transducer at an angle of 45°. The three optical fibers are placed 10 mm away from the center of the mirror plate, such that they are located in the focal zone of the ultrasound transducer. The diameter of the optical fibers is 140 μm and the pitches

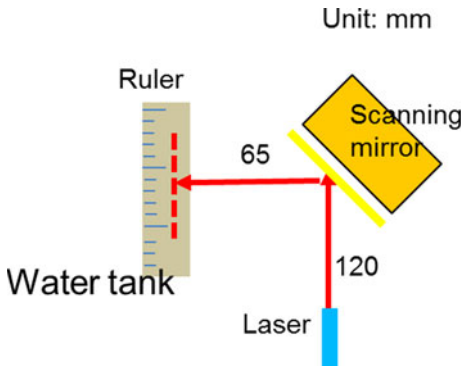

Fig. 4 Illustration of laser tracing method

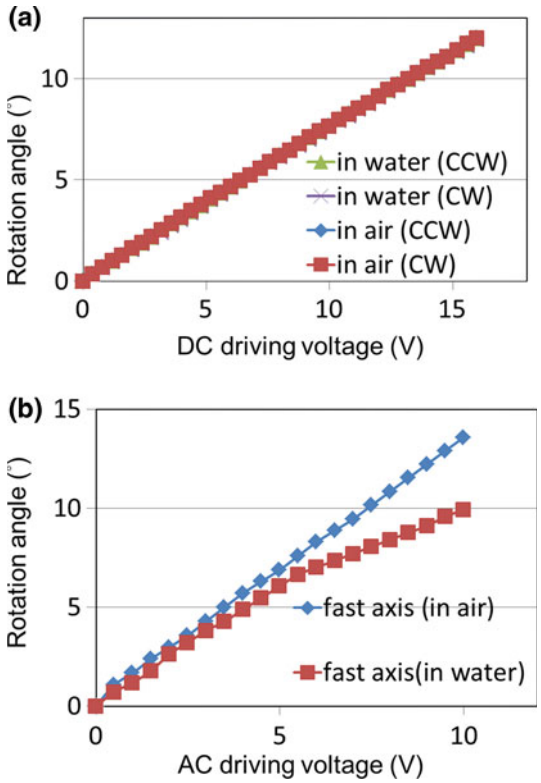

Fig. 5 Scanning angles of the fast axis of the water-immersible scanning mirror: **a** with a DC driving voltage; and **b** with an AC at the resonance frequency in air (224 Hz) and water (164 Hz). *CW* clockwise, *CCW* counter clockwise

between two adjacent fibers are 0.64 and 0.7 mm, respectively. The ultrasound transducer is connected to a pulser/receiver system (5072PR, Olympus) and an oscilloscope (TDX 2014B, Tektronix). The pulses repetition rate and pulse width were set to be 200 Hz and 1 μs, respectively. A DAQ card (PCI 6251, National Instruments) and a custom-built operational amplifier array were used to provide DC voltages to drive the two axes of the scanning mirror. The DC driving voltage of the fast axis was from −10 to

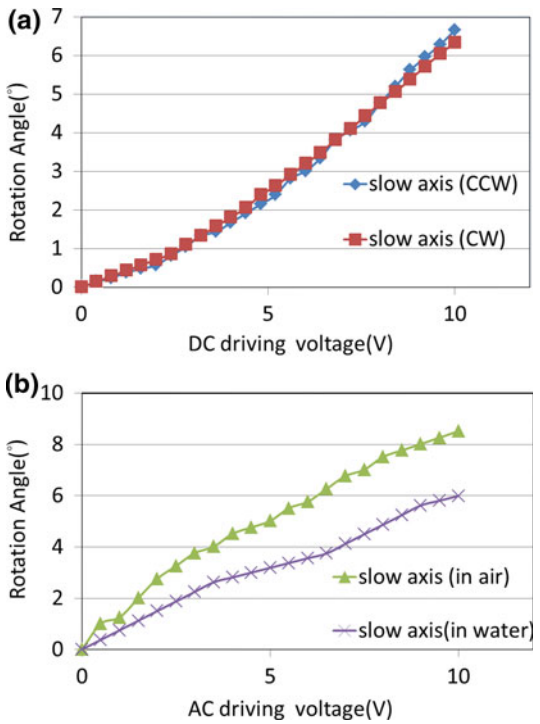

Fig. 6 Scanning angles of the slow axis of the water-immersible scanning mirror: **a** with a DC driving voltage; and **b** with an AC at the resonance frequency in air (55 Hz) and water (38 Hz). *CW* clockwise, *CCW* counter clockwise

10 V with a 0.4 V increment and that of the slow axis was from 0 to 8 V with a 0.4 V increment. This forms 1,000 scanning steps, corresponding to a scanning area of 0.8 mm × 2.6 mm with 20 × 50 pixels. At each "pixel", the peak-to-peak voltage of the received ultrasound signals were measured and averaged 128 times. To automate the scanning and data acquisition process, a Labview (National Instruments) program was developed to control the DAQ card and the oscilloscope. Figure 7b shows the normalized averaged peak-to-peak voltages as a function of the lateral and vertical scanning location. The distances between the three peaks of the backscattered ultrasound signals were 0.676 and 0.728 mm, respectively, which agreed well with the actual distances between the optical fibers.

5 Conclusion

In conclusion, we have demonstrated a new two-axis scanning mirror microsystem, which is specially designed for reliable and fast underwater scanning of both optical and ultrasonic beams. This unique feature can be potentially used to enhance the imaging capability of scanning acoustic microscopy and photoacoustic microscopy where a liquid matching medium is needed. Future work will focus on the optimization and further miniaturization of the

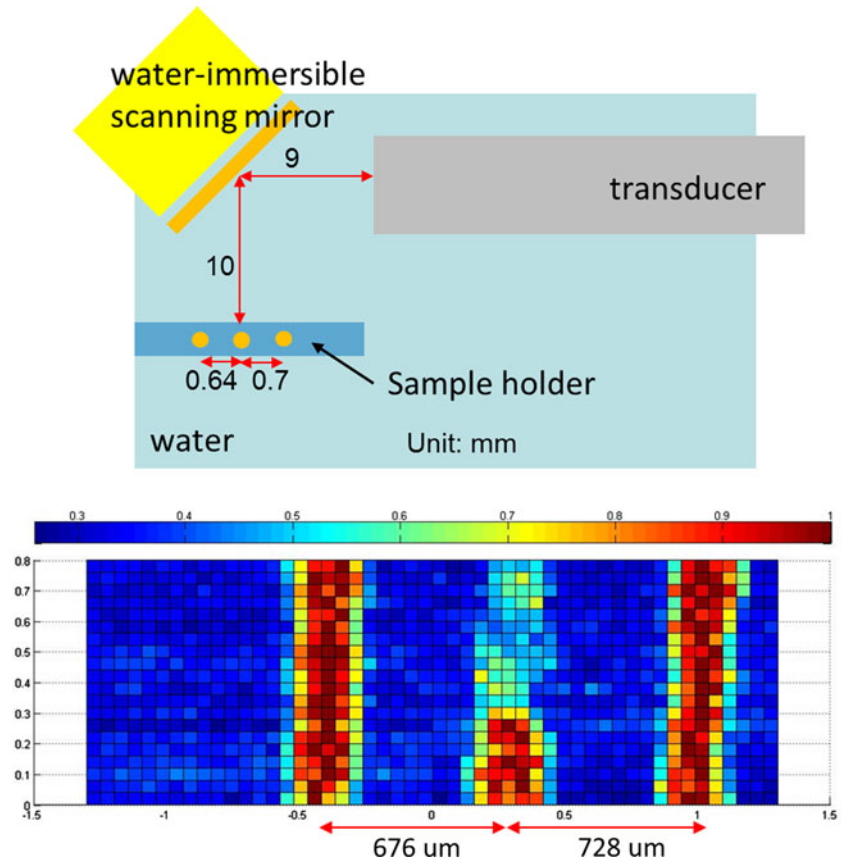

Fig. 7 **a** Schematic setup of the pulse/echo ultrasound microscopic imaging setup; and **b** averaged peak-to-peak voltage of the backscattered ultrasound signal as a function of lateral and vertical scanning location

scanning mirror microsystem and also its application in new ultrasound and photoacoustic microscopic imaging modalities.

Acknowledgments This work was supported in part by a grant from the National Institutes of Health (U54-CA136398) and a grant from the National Science Foundation (CMMI-1131758). Lihong Wang has a financial interest in Microphotoacoustics, Inc. and Endra, Inc., which, however, did not support this work.

References

Chen WH, Gottlieb EJ, Cannata JM, Chen YF, Shung KK (2000) Development of sector scanning ultrasonic backscatter microscope. 2000 IEEE Ultrasonics Symposium

Cornelis AVE, John ES (2006) Resonant frequencies of a rectangular cantilever beam immersed in a fluid. J Appl Phys 100:114916

Hagelin PM, Krishnamoorthy U, Heritage JP, Solgaard O (2000) Scalable optical cross-connect switch using micromachined mirrors. IEEE Photonics Technol Lett 12:882–884

Hyejun R, Piyawattanametha W, Taguchi Y, Daesung L, Mandella MJ, Solgaard O (2007) Two-dimensional MEMS scanner for dual-axes confocal microscopy. J Microelectromech Syst 16:969–976

Jung WY, Tang S, McCormic DT, Xie TQ, Ahn YC, Su JP, Tomov IV, Krasieva TB, Tromberg BJ, Chen ZP (2008) Miniaturized probe based on a microelectromechanical system mirror for multiphoton microscopy. Opt Lett 33:1324–1326

Liu C (2006) Foundations of MEMS. Upper Saddle River, NJ

Wang LV (2009) Multiscale photoacoustic microscopy and computed tomography. Nat Photonics 3:503–509

Wang L, Maslov K, Yao J, Rao B, Wang LV (2011) Fast voice-coil scanning optical-resolution photoacoustic microscopy. Opt Lett 36:139–141

Yang VXD, Mao YX, Standish BA, Munce NR, Chiu S, Burnes D, Wilson BC, Vitkin IA, Himmer PA, Dickensheets DL (2006) Doppler optical coherence tomography with a micro-electro-mechanical membrane mirror for high-speed dynamic focus tracking. Opt Lett 31:1262–1264

Yao J, Wang LV (2011) Photoacoustic tomography: fundamentals, advances and prospects. Contrast Media Mol Imaging 6:332–345

Yao J, Maslov KI, Zhang Y, Xia Y, Wang LV (2011) Label-free oxygen-metabolic photoacoustic microscopy in vivo. J Biomed Opt 16:076003